*Work supported by the U. S. Atomic Energy Commission.

[1]H. F. Helbig, D. B. Millis, and L. W. Todd, Phys. Rev. A 2, 771 (1970).

[2]H. H. Michels, J. Chem. Phys. 44, 3834 (1966).

[3]L. Wolniewicz, J. Chem. Phys. 43, 1087 (1965).

[4]L. D. Doverspike, R. L. Champion, S. M. Bobbio, and W. G. Rich, Phys. Rev. Letters 25, 909 (1970).

[5]G. Moliere, Z. Naturforsch. 2a, 133 (1947); L. I. Schiff, Phys. Rev. 103, 443 (1956); R. T. Glauber, *Lectures in Theoretical Physics* (Interscience, New York, 1958), Vol. 1, p. 315; R. G. Newton, *Scattering Theory of Waves and Particles* (McGraw-Hill, New York, 1966), p. 582.

[6]J. C. Y. Chen, C.-S. Wang, and K. M. Watson, Phys. Rev. A 1, 1150 (1970).

[7]J. C. Y. Chen and K. M. Watson, Phys. Rev. 174, 152 (1968); 188, 236 (1969).

[8]L. Wilets and S. J. Wallace, Phys. Rev. 169, 84 (1968).

[9]F. W. Byron, Jr., in Proceedings of the Sixth International Conference on the Physics of Electronic and Atomic Collisions, Cambridge, Mass., 1969 (unpublished). This has been derived analogously, independently, by the present author; it may also be obtained from the Schiff approximation for inelastic scattering: R. J. Cross, Jr., J. Chem. Phys. 47, 3724 (1967).

PHYSICAL REVIEW A VOLUME 4, NUMBER 1 JULY 1971

Energy Spectra of Metastable Oxygen Atoms Produced by Electron-Impact Dissociation of O_2 †

Walter L. Borst* and E. C. Zipf
Department of Physics, University of Pittsburgh, Pittsburgh, Pennsylvania 15213
(Received 18 January 1971)

Kinetic energies of metastable O atoms formed in dissociative excitation of O_2 were measured by a time-of-flight experiment. Metastable $O(^5S^0)$ atoms (9.14 eV) as well as high-lying states near the ionization limit of O (13.6 eV) were detected by means of Auger ejection of secondary electrons from a Cu-Be surface. The energy spectra of metastable fragments showed distinct structure with maxima near 0.3 and 2 eV. Repulsive-potential-energy curves of O_2 were constructed from the measured energy spectra and time-resolved excitation functions. The excitation function for the direct excitation of the $O(^5S^0)$ state had a threshold of 14.3 ± 0.2 eV which is equal to the minimum energy for dissociatively exciting the $O(^5S^0)$ state. Using selection rules and symmetry arguments concerning the angular variation of dissociation products, the molecular state reached near 14.3 eV was identified as a Π_u state with a probable multiplicity of 3. Other molecular states reached at higher energies were not identified. It seems, however, that there was a sizable contribution due to O atoms in high-lying Rydberg states excited in dissociative excitation. The differential cross section for the direct formation of $O(^5S^0)$ was found to be $d\sigma/d\Omega \simeq 1\times10^{-19}$ cm^2/sr within a factor of 2 at an electron energy of 30 eV and an angle of 90° with respect to the electron beam. Several atmospheric applications of the measurements concerning the heating of the atmosphere, radiative transfer of resonance radiation, and chemical reactions are mentioned briefly.

I. INTRODUCTION

Dissociation of molecular gases by electron impact is an important atmospheric collision (e.g., auroras). Dissociation of molecular oxygen is of particular interest, since metastable oxygen atoms play a dominant role in the earth's atmosphere. We have studied the dissociative excitation of high-lying metastable states of the O atom, in particular the O(5S) state. This state is readily excited with high efficiency. Low-lying metastable oxygen atoms are more difficult to detect and we are presently working on their dissociative excitation. In our apparatus, high-lying metastables and Rydberg atoms were observed perpendicularly to the electron-beam direction. Our measurements of energy spectra of metastables[1] resulting from dissociation of O_2 indicate that energetic atoms are formed with energies generally much above thermal. Energy spectra of metastable atoms also need to be known in absolute cross-section determinations of long-lived emissions excited in the dissociation process.

The technique used involved the pulsed production of metastables and multichannel analysis of their time-of-flight spectra, and has already been described in detail.[2] Only the salient features of the apparatus are mentioned below.

II. EXPERIMENTAL DETAILS

The experimental system has been described elsewhere.[2] It suffices to mention the main features of the apparatus (Figs. 1 and 2).

Metastable oxygen atoms were produced by electron-impact dissociation of O_2. The electron gun

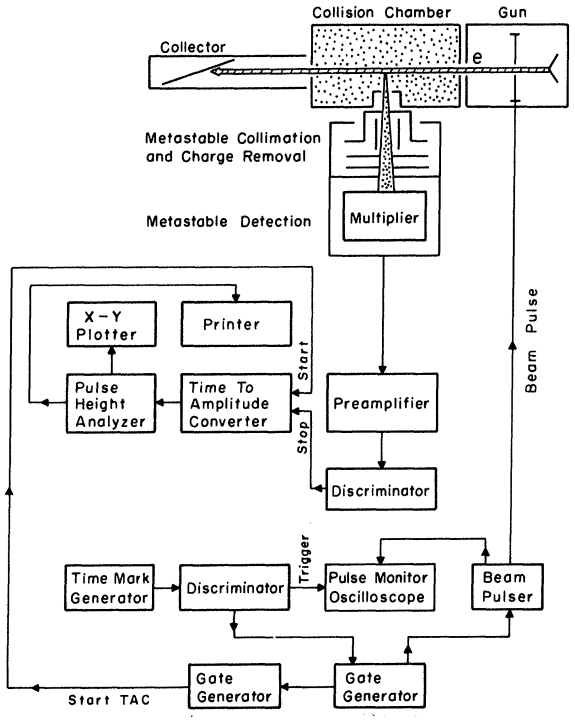

FIG. 1. Schematic diagram of apparatus involving time-to-amplitude conversion for measuring time-of-flight distributions.

was pulsed in order to monitor the transit time of metastables to the detector and thus obtain time-of-flight distributions of metastable fragments. Beam pulses were typically 1 μsec wide with repetition rates of 10^4/sec. The duty cycle of the gun was thus 1% and the average beam current as integrated by an electrometer was about 10^{-7} A.

Metastable fragments were detected under an angle of 90° with respect to the beam direction by a nude Cu-Be multiplier whose first dynode was 6.4 cm away from the center of the collision chamber. The solid angle subtended by the multiplier entrance aperture was about 0.05 sr. The effective scattering length in the collision chamber was about 0.5 cm. The collision chamber containing the O_2 gas at an uniform pressure ($\sim 10^{-4}$ Torr) represented a diffuse gas source.

Metastables with excitation energies in excess of the work function of the multiplier dynodes ($\phi \sim 4$ eV) could liberate secondary electrons from the multiplier dynodes by means of the Auger process.[3] Therefore the $3s^5S^0$ state and high-lying Rydberg states of atomic oxygen could be detected. It is interesting to note that metastable oxygen molecules were never detected in this experiment. Total counting rates at the detector integrating over all metastable transit times were of the order of 100/sec. The background counting rate without O_2 in the collision chamber was about 0.1/sec.

Time-of-flight spectra of metastable atoms (Figs. 3 and 4) were obtained with a multichannel-analyzer system involving time-to-amplitude conversion (Fig. 1) or with a single-channel analyzer of variable channel width and position (Fig. 2). In the first method (Figs. 1 and 3), the data were taken automatically, the statistics were better, and the drifts were negligible. The second method (Figs. 2 and 4) enabled one to obtain excitation functions for groups of metastables with selected transit times, i.e., kinetic energies, by the proper choice of the gating-window position and width. In this case, the output of a ratemeter parallel to the counter in Fig. 2 was applied to an x-y recorder together with the energy-defining voltage of the electron gun.

III. RESULTS

A. Energy Spectra

Time-of-flight spectra of metastable O atoms are shown in Figs. 3 and 4. Originally these spectra (Fig. 4) were obtained with the single-channel analyzer sketched in Fig. 2. The multichannel-analyzer system (Fig. 1) yielding the spectra in Fig. 3 was added at a later date in order to facilitate the

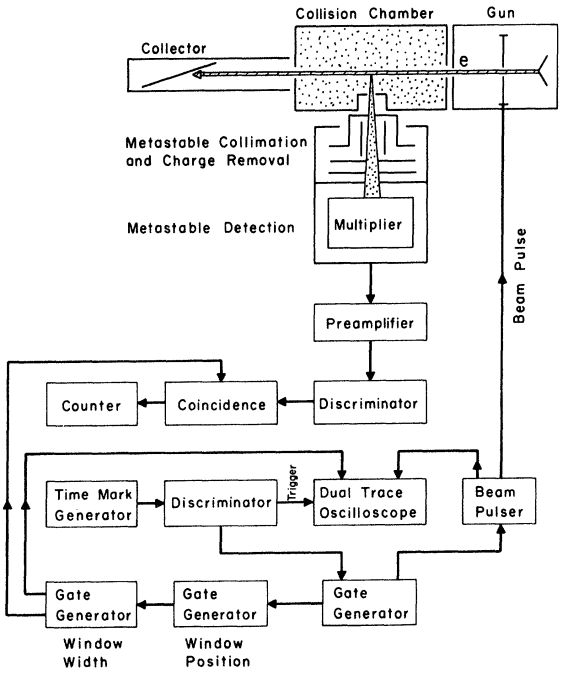

FIG. 2. Schematic diagram of apparatus using single-channel analysis of time-of-flight distributions. The system was also utilized to measure time-resolved excitation functions by either using a ratemeter x-y recorder combination or a multichannel scaler parallel to the counter.

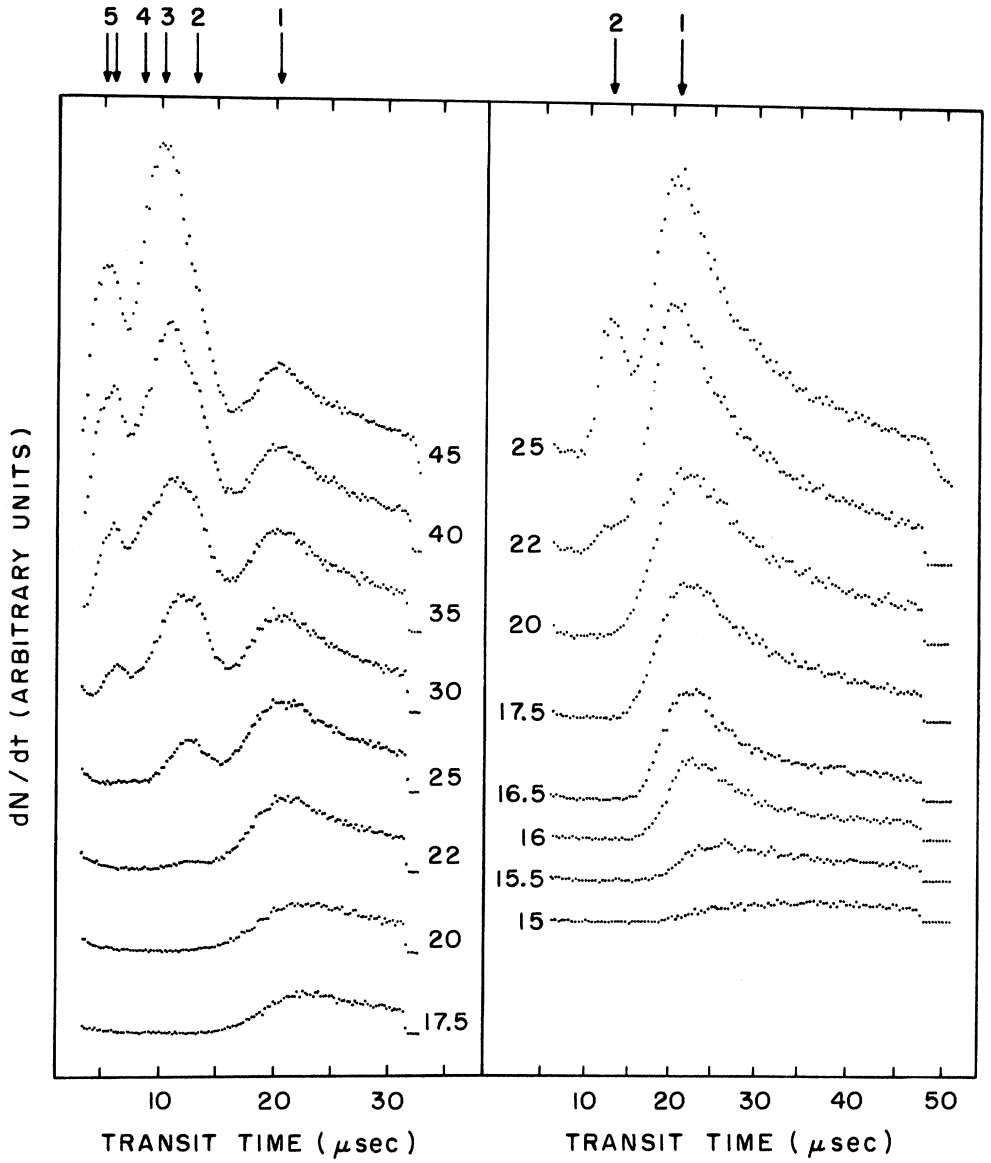

FIG. 3. Multichannel-analyzer plots of time-of-flight distributions of metastable oxygen atoms. Discernible structure is numbered 1–5. The zero lines of the distributions are indicated by horizontal dots on the right. The left half of the figure shows distributions obtained for electron energies up to 45 eV whereas the right half emphasizes the low-energy domain.

data taking and to improve the over-all accuracy. It is seen that the agreement between the data in Figs. 3 and 4 is very good if one takes into account the lower time resolution in Fig. 4. All curves were due to relatively fast O metastables. Molecular oxygen metastables would have had much longer transit times and a detailed search for them never revealed their presence in our experiment.

Pronounced structure in the time-of-flight distributions is indicated by arrows in Fig. 3. The threshold for metastable production is somewhat below 15 eV. As the electron energy increases, structure 1 develops fully and remains constant in shape, while at the same time further structure appears. As discussed below, the structure in the time-of-flight distribution contains important information about the molecular structure of O_2.

Energy spectra of metastable atoms resulting from the dissociation process are of practical as well as basic interest. These spectra were obtained from the corresponding time-of-flight distributions in the following way: Let $T_E(t)$ be the time-of-flight distribution of metastables produced at an electron energy E. Then the signal accumulated in

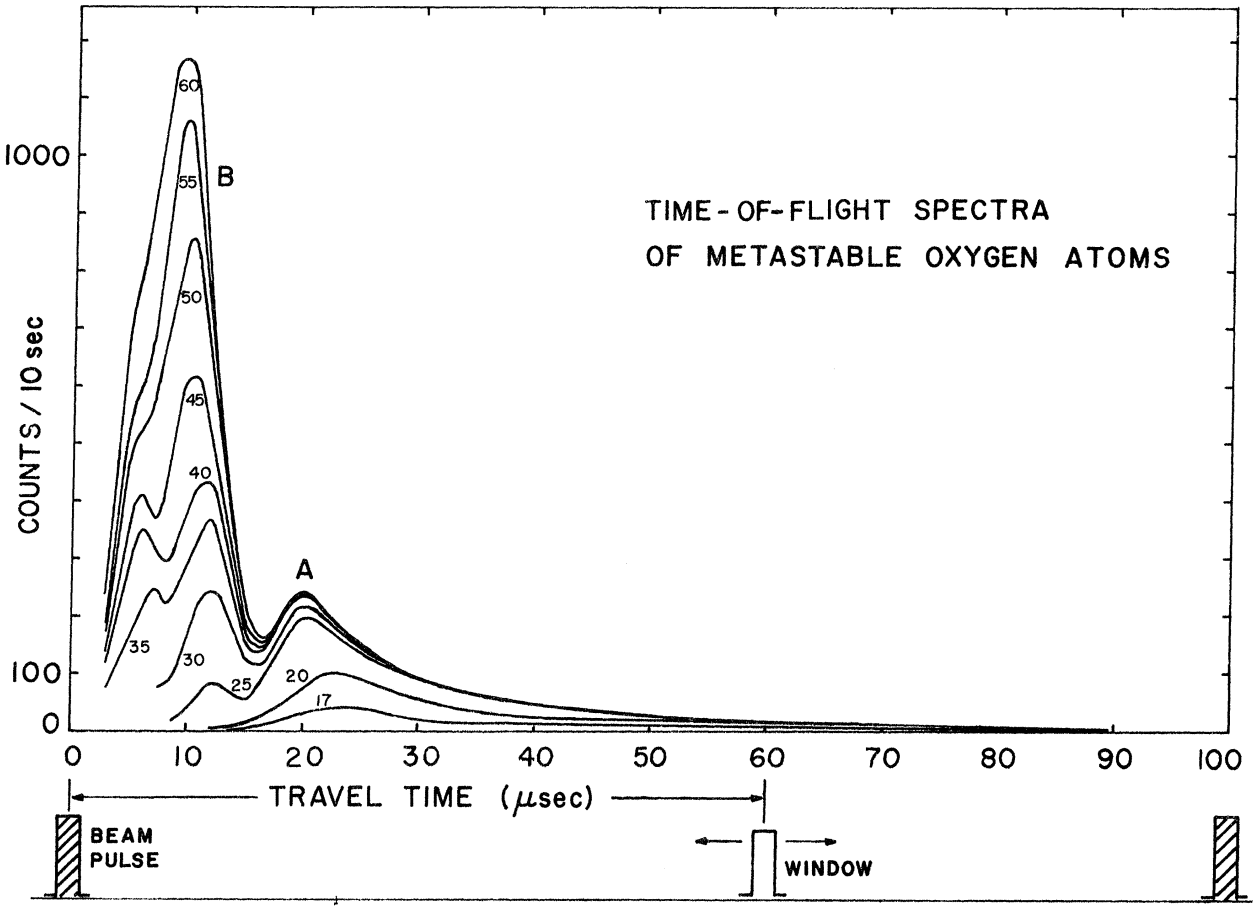

FIG. 4. Time-of-flight distributions obtained with the single-channel analyzer (Fig. 2). The distributions are similar to those in Fig. 3 except for lower resolution due to a 2-μsec width of the counting window. The parameter on the curves is the electron energy.

the analyzer is proportional to $T_E(t)\,dt$, where dt is the transit time interval given by the channel width (~ 0.2 μsec). The energy spectrum $D_E(\epsilon)$ corresponding to the distribution $T_E(t)$ is then obtained by using

$$\epsilon = \tfrac{1}{2} Md^2/t^2 , \tag{1}$$

which gives

$$T_E(t)\,dt = -(1/Md^2)T_E(t)t^3\,d\epsilon . \tag{2}$$

From this expression we see that the energy spectrum (aside from an insignificant constant factor) is given by

$$D_E(\epsilon) = T_E(t)t^3 , \tag{3}$$

where ϵ is the kinetic energy per metastable fragments, M the mass of O, d the distance between excitation region and metastable detector, and t the metastable transit time.

In the actual calculation of energy spectra, the time-of-flight distributions were first multiplied by t^3 according to Eq. (3) and the product was plotted as a function of the energy ϵ. Computer plots of the resulting energy spectra are shown in Fig. 5. The low-energy portion in Fig. 5 corresponds to structure 1 in Fig. 3, the broad peak with a maximum near 2 eV corresponds to the combined structures 2, 3, and 4. Structure 5 shows up as a small pedestal at the higher energies in Fig. 5. The continued rise in the energy spectra below the inflection point at about 0.5 eV was caused by a very small constant background in the time-of-flight distributions. Clearly, even the smallest background will cause the energy spectra to diverge eventually at the lowest energies (longest transit times) according to Eq. (3). In order to assess this background properly, data extending to very long transit times and containing good statistics were taken. This enabled one to subtract any background. An energy distribution obtained in this way at 20 eV is shown in Fig. 6. It is clear from this figure that the energy spectrum reaches a maximum

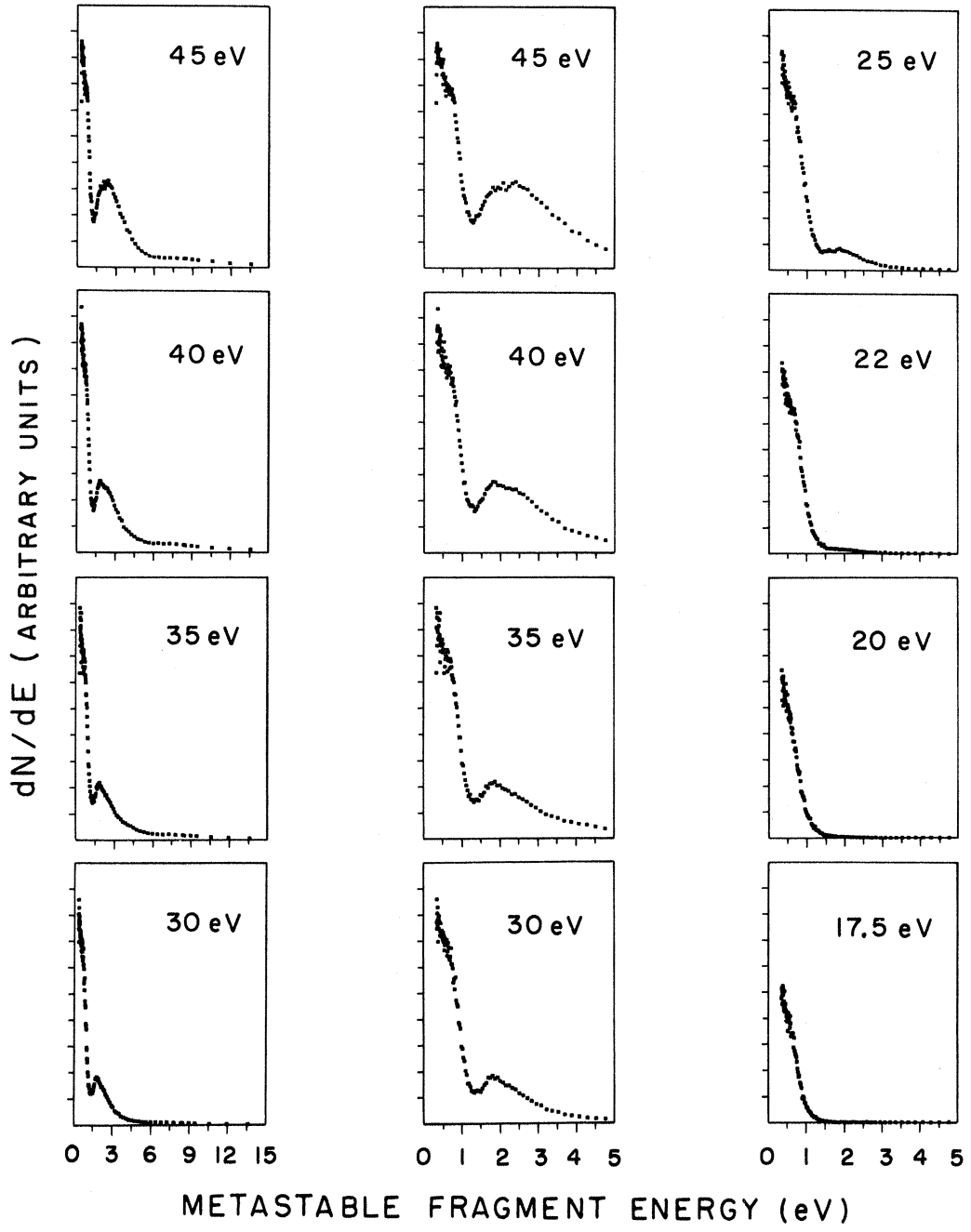

FIG. 5. Energy spectra of metastable oxygen atoms obtained from time-of-flight distributions such as in Fig. 3. The kinetic energy per metastable atom is listed on the abscissa. Distinct structure is observed around 0.5 and 2 eV. The rise in the spectra below 0.5 eV is due to a very small background in the time-of-flight distributions (see also Fig. 6).

somewhat below 0.5 eV and a constant value at zero kinetic energy. Only the lowest-energy portion of the spectra in Fig. 5 was affected by the small background in the time-of-flight distribution, whereas the portion above about 0.5 eV remained unaffected.

In arriving at the energy spectra in Figs. 5 and 6, the velocity distribution of the parent oxygen molecules and metastable recoil after the electron collision were neglected. It has been shown[2] that metastable recoil for a diffuse gas source should be rather negligible, especially in the present experi-

ment where metastable energies are above thermal. It was estimated, however, that the velocity distribution of the parent molecules could cause a broadening in the energy and time-of-flight spectra of the order of 30%. Some further broadening was also caused by the necessarily finite width (~1 μsec) of the electron gun pulse. This finite beam pulse width affects the high-energy part of the spectra more than the low-energy part, whereas the reverse is true for the effect of the energy distribution of the parent molecules. It was decided, however, that for the purposes of this paper no additional physical insight would be gained by using unfolding techniques and eliminating the broadening indicated above.

B. Kinetic Energy Effects on Secondary Electron Yield

As long as the metastable fragment energy remained below the work function of the Cu-Be multiplier dynodes ($\phi \gtrsim 4$ eV), there was no way in which secondary electrons could be ejected by virtue of the *kinetic* energy of the metastables. It is seen in Figs. 5 and 6 that the main part of the energy spectra is well below 4 eV. Even as the kinetic energy increases to several eV above the work function, the kinetic yield γ_{kin} can be expected to be small compared with the yield γ_{pot} for the ejection of secondary electrons due to the potential (excitation) energy of the metastables.[4] However, the problem remains that the yield γ_{pot} itself may depend on the kinetic energy of the metastables both below and above the work function. If this is indeed the case, then the measured spectra would be distorted by the energy dependence of γ_{pot}. It is to be noted that Hagstrum's measurements[5] of the secondary electron yield of rare-gas ions with energies above 5 eV on tungsten surfaces show some energy dependence of the yield. If his measurements are extrapolated linearly to zero energy, then the variation of the yield in the energy range 0–5 eV should indeed be small. But it is uncertain whether such an extrapolation is valid and whether it applies to metastable oxygen atoms on a contaminated Cu-Be surface. Since there does not seem to be any definite answer to this problem, we have assumed a constant yield for all metastable kinetic energies in question.

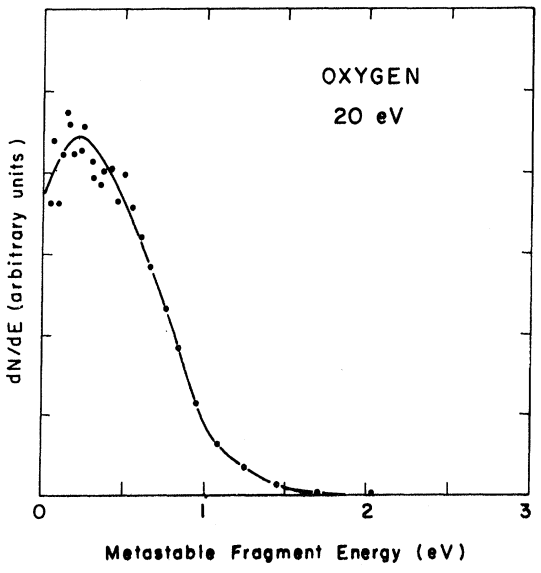

FIG. 6. Energy spectrum of oxygen metastables produced at 20-eV electron energy. The small background in the corresponding time-of-flight distribution was carefully assessed and subtracted. Note that the energy distribution is finite at zero kinetic energy.

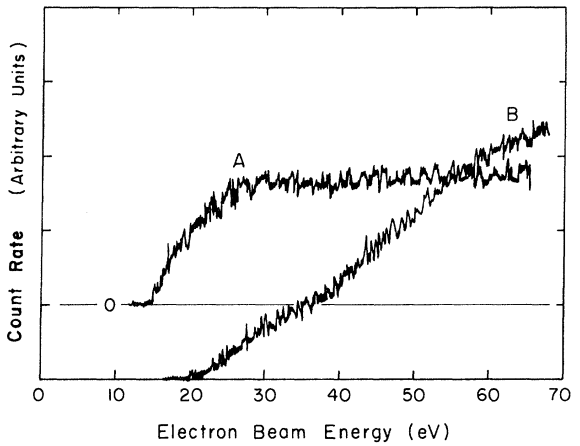

FIG. 7. Time-resolved excitation functions for dissociative excitation of metastable oxygen atoms. Curves A and B correspond to the excitation of structures A and B in Fig. 4, respectively. The counting window (Fig. 4) for curve A extended from 14 to 55 μsec and for curve B from 6 to 14 μsec.

C. Excitation Functions

Further information about the process of dissociative excitation could be obtained by monitoring excitation functions for the production of metastables with selected kinetic energies. Figure 7 shows excitation functions corresponding to the two distinct features at higher and lower kinetic energies in Figs. 4 and 5. Excitation function A in Fig. 7, which corresponds to the less energetic portion of metastables, has a threshold of 14.3 ± 0.2 eV. This agrees, within limits of error, with the minimum energy (14.3 eV) required for dissociatively exciting the metastable $O(^3s\,^5S)$ state, whose excitation energy is 9.14 eV. Curve A in Fig. 7 remains constant for energies above 30 eV. In distinction to this, curve B in Fig. 7, which represents the more energetic fraction of metastables, has a higher-ly-

ing threshold near 21 eV, shows a break near 39 eV, and reaches a maximum (not shown) somewhat above 100 eV. The implications of the structure in the energy spectra and excitation functions are discussed in Secs. IV and V.

D. Absolute Cross Sections

Metastable oxygen atoms were produced with relatively large efficiencies. It was possible to estimate the absolute cross section for production of $O(^5S)$ atoms by integrating the signal over structure A in Fig. 4 from about 15 to 55 μsec using the single-channel analyzer (Fig. 2) and monitoring the resulting excitation function (curve A in Fig. 7).

The counting rate at the metastable detector was given by

$$C = \frac{I_b}{e} nl \frac{d\sigma}{d\Omega} \Delta\Omega \gamma_m , \tag{4}$$

where I_b is the electron beam current, e the electronic charge, n the O_2 density, l the effective scattering length of the collision chamber, $\Delta\Omega$ the solid angle subtended by the detector at the center of the collision chamber, γ_m the secondary yield for $O(^5S)$ atoms on Cu-Be, and $d\sigma/d\Omega$ the differential cross section at an angle 90° with respect to the electron beam. All quantities in Eq. (4) except γ_m and $d\sigma/d\Omega$ were known rather accurately.

As will be discussed elsewhere, a value of $\gamma_m \sim 0.01$ can be assumed for $O(^5S)$ atoms within a factor of 2 by comparing secondary yields for various metastable atoms and molecules. This yields a cross section of

$$d\sigma/d\Omega \simeq 1\times10^{-19} \text{ cm}^2/\text{sr} \tag{5}$$

at an angle of 90° and an electron energy of 30 eV (flat part of curve A in Fig. 7). It is very likely that the differential cross section is not isotropic with respect to the scattering angle. Nonetheless it can be expected that the total cross section integrating over all angles is close to 10^{-18} cm^2. This value applies to structure A in Fig. 4 alone and thus to the less energetic fraction of metastables (Fig. 6). The total cross section for all high-lying metastables including long-lived Rydberg atoms, i.e., for the combined structures A and B in Fig. 4, is of course larger. Taking into account the larger secondary electron yield for higher-lying states, and assuming that these states are indeed long-lived enough for direct detection, it was estimated that the maximum cross section for all high-lying states is of the same order of magnitude as that for the $^5S^0$ state. It is to be noted that the two low-lying ^1D and ^1S metastable states of O did not contribute in the present measurements.

IV. DISCUSSION

A potential-energy diagram derived from our measurements is shown in Fig. 8. It is seen that the energy spectra of the atomic fragments[6] determine the shape of the repulsive part of the potential curves. The positions of the potential curves with respect to the energy axis were determined by the onsets in the two excitation functions at 14.3 and about 21 eV (Fig. 7). The construction of the repulsive curves from the ground-state prob-

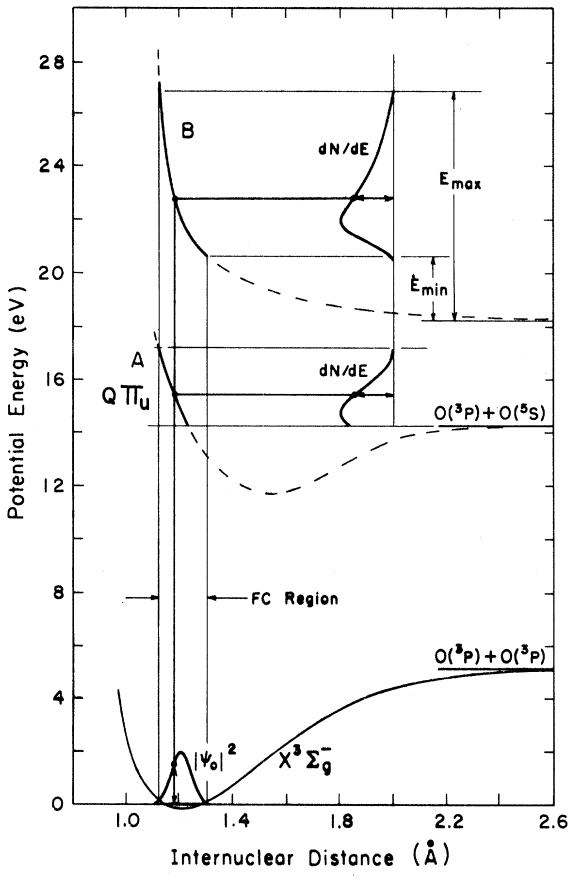

FIG. 8. Semiquantitative representation of potential-energy curves resulting from the two main features in the energy spectra around 0.5 and 2 eV (Figs. 5 and 6). It is seen that a finite value of the energy spectrum at zero kinetic energy is indicative for dissociation from the repulsive part of a bound curve. Dissociation from a purely repulsive curve leads to a zero value of the energy spectrum at a finite kinetic energy E_{min}. The construction of the potential curves from the energy spectra and the probability distribution $|\psi_0|^2$ of the ground state is shown. The dashed portions of the potential curves between the Franck-Condon region and the dissociation limits are rather arbitrary. The purely repulsive curve was obtained from the 30-eV measurements and is qualitative. Several states may have contributed to this curve. Furthermore, an uncertainty of about 0.5 eV existed in the excitation threshold of structure B (Figs. 4 and 7) and thus also in the dissociation limit. The bound curve corresponds to dissociative excitation of the $O(^5S)$ state near the minimum threshold of 14.3 eV.

ability function $|\Psi_0|^2$ and the energy spectra dN/dE (normalized to the same maximum height as $|\Psi_0|^2$) is evident in Fig. 8. It was assumed that the Franck-Condon principle holds near threshold and that the wave functions appropriate for the repulsive-potential curves can be closely approximated by δ functions.[7]

There can be little doubt that the low-energy spectrum leading to curve A in Fig. 8 corresponds to the $O(^5S)$ state alone because of the observed threshold near 14.3 eV and the fact that the energy spectrum (Fig. 6) extends down to zero kinetic energies having a finite value there. Even at the higher electron energies above threshold, the $O(^5S)$ state seems to be produced directly with a rather negligible cascade contribution. The reason for this is that the low-energy spectra (Fig. 6) remain essentially constant in shape with varying electron energy and the excitation function A in Fig. 7 shows no discernible structure. In contrast to this, the high-energy portion of metastables is more difficult to interpret. There exists a minimum nonzero fragment energy $E_{\min}$ (Fig. 8), which, together with the onset in the excitation function B (Fig. 7) near 21 eV, yields a dissociation limit of about 18.5 eV or slightly less. This energy is very close to the threshold for dissociative ionization ($\sim$ 18.6 eV) and definitely above that for direct excitation of the $O(^5S)$ state. It seems that O atoms in highly excited (Rydberg) states are produced with lifetimes sufficiently long ($\gtrsim 10$ μsec) for direct detection. It is possible that some of these highly excited states just below the ionization limit of O cascade down to the $O(^5S)$ state.

The formation of highly excited O atoms in electron-impact dissociation was also observed by Kuprianov,[8] who detected these atoms by surface, field, and Penning ionization. The $O(^5S)$ state, however, had too low an excitation energy to be observed by these methods. It is very interesting to note that curve B in Fig. 7 for the process

$$O_2 + e \rightarrow O^{**} + O + e \qquad (6)$$

is very similar to that obtained by Kuprianov for the dissociative ionization process

$$O_2 + e \rightarrow O^+ + O + 2e. \qquad (7)$$

This indeed suggests that highly excited O^{**} atoms are formed in Rydberg states which converge to the proper O^+ ionization limit.

It is seen from the structure numbered 2, 3, and 4 in the time-of-flight spectra (Fig. 3) that several states contributed. This makes a detailed interpretation somewhat uncertain. Furthermore, additional structure 5 in Fig. 3 appears at high electron energies. It was found that this structure disappeared as the detector distance was increased from 6 to about 22 cm. This indicates that the lifetime of excited fragment atoms in this case was of the order of 10 μsec or less. In distinction to this, the relative peak heights of structure 1 and the group represented by structures 2, 3, and 4 remained practically constant, and there was no decay as the detector distance was increased. This indicates that the excited atoms produced in this case have long lifetimes. In fact, the lifetime of the $O(^5S)$ state can be expected to be about 600 μsec.[9] The lifetime of Rydberg states is also of the same order if the principal quantum number n is about 10 or higher.[10]

In the following we concentrate on our results for O atoms produced in the ^5S state. Here the ambiguities in the interpretation are rather few in contrast to the case of higher-lying states.

V. ASSIGNMENT OF STATES

It was possible to determine the state of O_2 which led to structure 1 and A in Figs. 3 and 4, respectively, and to excitation function A in Fig. 7. It was established from the threshold in the excitation function near 14.3 eV, together with the shape of the energy spectrum (Fig. 6) which extended to zero kinetic energies, that the dissociation products were $O(^5S^0) + O(^3P)$. Cascading to the $O(^5S^0)$ state must have played a minor role since structure in the excitation function was absent and the shapes of the time-of-flight and energy distributions were constant for electron energies sufficient to cover the Franck-Condon region (Fig. 8), i.e., energies above 18 eV. Therefore, one state of O_2 was probably responsible for the observed direct formation of $O(^5S^0)$. Using symmetry arguments given for example by Herzberg,[7] this state was identified in the following way: The states $S^{\text{odd}} + P^{\text{even}}$ of the separated O atoms lead to possible molecular states $\Sigma^+_{u,g}$ and $\Pi_{u,g}$ of O_2. However, the $\Sigma^+_{u,g}$ states can be excluded since O_2 has a $^3\Sigma^-_g$ ground state and the transition $- \longleftrightarrow +$ is highly forbidden in electron-impact excitation according to Lassettre and Krasnov.[11] We can further exclude Π_g states because the matrix element for the transition $\Sigma^-_g \rightarrow \Pi_g$ vanishes in the Born approximation for an observation angle of 90° (and 0°) with respect to the beam direction according to Dunn.[12] On the other hand, the matrix element for the transition $\Sigma^-_g \rightarrow \Pi_u$ is nonzero for an angle of 90° (and zero for 0°). Although the Born approximation is not valid near threshold, we assumed that the molecular state in question is a Π_u state nonetheless, since there was a sizable signal at higher energies where this approximation should yield correct results. From the multiplicity of the dissociation products it follows that the Π_u state has the multiplicity 3, 5, or 7. A multiplicity of 7 can be excluded because it would require a double spin flip. It is most likely that the Π_u state has a multiplicity of 3 because it is ex-

cited with appreciable strength at higher electron energies. For a change in multiplicity, excitation functions usually drop off distinctly at the higher energies, in contrast to our measurements (see curve A in Fig. 7). We cannot exclude the possibility that there was a $^5\Pi_u$ state contribution at the lowest energies. We have designated the $^3\Pi_u$ as a $Q^3\Pi_u$ state, where the letter Q indicates that the oxygen quintet S state is formed in the dissociation process.

We did not attempt to identify the states leading to the more energetic group of metastable fragments (Fig. 5 and structures 2–5 in Fig. 3). The dissociation products were not known in this case and furthermore several states contributed. The purely repulsive-potential curve drawn in Fig. 8 is only qualitative and is an average over at least two states which contributed at an electron energy of 30 eV.

VI. SUMMARY AND CONCLUSIONS

(i) We have observed groups of O metastables produced in electron-impact dissociation of O_2 with mean kinetic energies of about 0.3 and 2 eV. Metastable O atoms were formed in the $O(^5S)$ state (9.14 eV) as well as high-lying Rydberg states near the O ionization limit.

(ii) The energy spectra of metastables together with time-resolved excitation functions were used to construct repulsive-potential-energy curves of O_2.

(iii) The $O(^5S)$ state was produced near the minimum energy of 14.3 eV required for its dissociative excitation. On the basis of selection rules and symmetry arguments concerning the angular variation of metastable fragments, the molecular state having the dissociation limit $O(^5S)+O(^3P)$ at 14.3 eV was identified as a $^3\Pi_u$ state with some uncertainty in the multiplicity. Keeping in mind the dissociation product $O(^5S)$, we have called this state the $Q^3\Pi_u$ state, where Q stands for quintet. We have not attempted to identify molecular states reached at higher energies. It is clear, however, that some of these molecular states lead to dissociation limits involving O atoms in high-lying (Rydberg) states.

(iv) The absolute differential cross section $d\sigma/d\Omega$ for the production of the $O(^5S)$ state was found to be 1×10^{-19} cm^2/sr within a factor of 2 at an electron energy of 30 eV and a direction perpendicular to the electron beam.

(v) Some geophysical implications of the present measurements are the following: The relatively high kinetic energies of metastables produced in dissociative excitation contribute to the heat input into the upper atmosphere, in particular under auroral conditions. Further, the nonthermal velocities of the fragments have to be taken into account in the radiative transfer treatment of resonance radiation of O and other species, since it is likely that ground-state atoms produced in dissociation of molecules have also nonthermal velocities. Finally, certain chemical reactions between dissociative fragments and atmospheric gases may be possible by virtue of either the high translational energies or the excitation energies of the fragments formed in the dissociation process.

ACKNOWLEDGMENT

We wish to thank sincerely P. W. Erdman for his helpful assistance in the data reduction.

---

†Work supported by NASA under Contract No. NGL 39-011-030 and by the Advanced Research Project Agency under Contract No. DA-31-124-ARO-D-440.

*Present address: Department of Physics, Southern Illinois University, Carbondale, Ill. 62901.

[1]W. L. Borst and E. C. Zipf, Bull. Am. Phys. Soc. 16, 205 (1971). At this meeting R. S. Freund presented results in close agreement with ours.

[2]W. L. Borst and E. C. Zipf, Phys. Rev. A 3, 979 (1971).

[3]H. D. Hagstrum, Phys. Rev. 96, 336 (1954).

[4]P. J. MacVicar-Whelan and W. L. Borst, Phys. Rev. A 1, 314 (1970).

[5]H. D. Hagstrum, Phys. Rev. 104, 1615 (1956).

[6]Note that the total kinetic energy of the two oxygen atoms after dissociation is very nearly twice that of each metastable fragment. This total energy was used in the construction of repulsive-potential curves in Fig. 8.

[7]G. Herzberg, *Spectra of Diatomic Molecules*, 2nd ed. (Van Nostrand, Princeton, N. J., 1950).

[8]S. E. Kuprianov, Zh. Eksperim. i Teor. Fiz. 55, 460 (1968) [Sov. Phys. JETP 28, 240 (1969)].

[9]R. H. Garstang, Proc. Cambridge Phil. Soc. 57, 115 (1961).

[10]H. Hotop and A. Niehaus, J. Chem. Phys. 47, 2506 (1967).

[11]E. N. Lassettre and M. E. Krasnov, J. Chem. Phys. 40, 1248 (1964).

[12]G. H. Dunn, Phys. Rev. Letters 8, 62 (1961).